



# Polyurethane-Based Elastomeric Polymer Electrolyte for Lithium Metal Polymer Cells with Enhanced Thermal Safety

Hyebeen Son, Hyun-Sik Woo, Myung-Soo Park, Ji Yun Min,\* and Dong-Won Kim<sup>\*,z</sup> 

Department of Chemical Engineering and Institute of Nano Science and Technology, Hanyang University, Seongdong-Gu, Seoul 04763, Korea

A large number of applications such as mobile electronics and electric vehicles requires rechargeable batteries with high energy density and enhanced safety. To achieve these goals, lithium metal batteries employing solid-state electrolytes have become common despite the safety concerns associated with lithium metal. Polymer electrolytes have been studied as a solution for enhancing the safety of lithium metal batteries because they are non-volatile, non-flammable, and suppress the growth of lithium dendrites. In this study, highly elastic polyurethane (PU)-based polymer electrolytes were prepared in the form of thin flexible films, and their electrochemical characteristics were investigated. To improve the ionic conductivity, non-volatile and non-flammable 1-ethyl-3-methylimidazolium bis(trifluoromethanesulfonyl)imide was added as a plasticizing additive to the polymer electrolyte. The cell assembled using a Li anode, PU-based elastomeric polymer electrolyte and composite  $\text{LiNi}_{0.6}\text{Co}_{0.2}\text{Mn}_{0.2}\text{O}_2$  cathode exhibited stable cycling performance by suppressing the growth of lithium dendrites as well as maintaining good interfacial contacts between electrolyte and electrodes during repeated cycling.  
© 2020 The Electrochemical Society ("ECS"). Published on behalf of ECS by IOP Publishing Limited. [DOI: 10.1149/1945-7111/ab8ed2]

Manuscript submitted March 5, 2020; revised manuscript received April 21, 2020. Published May 8, 2020.

Supplementary material for this article is available [online](#)

The demand for rechargeable batteries as energy storage devices has remarkably increased as regulations regarding use of fossil fuels have become stricter than ever before. In particular, large-scale batteries for various applications such as electric vehicles and energy storage systems are expected to dominate the future market, requiring higher energy density than current lithium-ion batteries (LIBs).<sup>1–6</sup> A lot of research has been performed to develop batteries with higher energy densities.<sup>6–10</sup> Replacing conventional anode materials such as graphite with lithium metal is a possible solution for achieving higher energy density, since lithium metal has a high theoretical specific capacity of  $3,860 \text{ mAh g}^{-1}$ . However, employing lithium metal as an anode material has been hindered by its high reactivity toward liquid electrolytes and occurrence of uncontrollable dendrite growth during charge and discharge cycles, which leads to internal short circuit, failure and eventually explosions. To overcome these problems, numerous strategies have been studied, such as the utilization of stable solid electrolyte interphase-forming additives,<sup>11,12</sup> protective coating on the lithium metal or separator,<sup>13–15</sup> and use of solid electrolytes.<sup>15–18</sup> Especially, the solid-state lithium batteries using solid electrolytes can be a fundamental solution to suppress the growth of lithium dendrite and avoid harmful reactions of liquid electrolyte at the surface of the lithium electrode.<sup>15–20</sup> Among the various types of solid electrolytes, polymer electrolytes have attractive properties including no leakage problems, non-flammability, easy processing for thin films, low cost, design flexibility, modifiable shapes and good interfacial contacts with electrodes. To date, solid polymer electrolytes based on poly(ethylene oxide) (PEO) have been actively studied for lithium metal batteries due to their strong solvating properties and high chain flexibility.<sup>21–25</sup> However, they show poor ionic conductivity at room temperature due to their highly crystalline nature. Moreover, the low anodic stability at high voltage shifted research interest to polymer electrolytes based on non-PEO polymers.<sup>26–34</sup> They provided great improvements in ionic conductivity and electrochemical stability as compared to those of PEO-based solid polymer electrolytes. However, their mechanical properties are often poor, and thus thin, free-standing films could not be obtained without a supporting membrane or additional thermal curing processes.

In our study, polyurethane (PU)-based thermoplastic elastomer was used for preparing highly elastic and free-standing polymer electrolytes, and their electrochemical and mechanical properties

were investigated. To improve ionic conductivity, a small amount of 1-ethyl-3-methylimidazolium bis(trifluoromethanesulfonyl) imide was added to the polymer electrolyte, since ionic liquid is non-flammable and non-volatile.<sup>35,36</sup> The obtained elastic polymer electrolyte showed good mechanical strength due to the phase-separated structure of the hard and soft segments of polyurethane. The flexible and elastic nature of the polymer electrolyte helped maintain good interfacial contacts between polymer electrolyte and electrodes. These unique properties enabled fabrication of a lithium metal polymer cell composed of a lithium anode and a composite  $\text{LiNi}_{0.6}\text{Co}_{0.2}\text{Mn}_{0.2}\text{O}_2$  cathode without a separator, and the cycling performance of the cells employing the elastic polymer electrolyte was evaluated.

## Experimental Methods

**Preparation of elastomeric polymer electrolytes.**—The solution casting method was used to prepare the polymer electrolyte as a thin film, as schematically illustrated in Fig. 1. As presented in Table I, appropriate amounts of thermoplastic PU elastomer (PU K-480A, KOLON Industries), lithium bis(trifluoromethanesulfonyl)imide (LiTFSI, PANAX ETEC), and 1-ethyl-3-methylimidazolium bis(trifluoromethanesulfonyl)imide (EMImTFSI, SOLVIONIC) were dissolved in anhydrous tetrahydrofuran (THF, Tokyo Chemical Industry). An optimized mass ratio (PU: LiTFSI = 1:1) was used in preparing the polymer electrolyte, since the composition exhibited high ionic conductivity and it was easy to obtain the free-standing film. The mixed solution was stirred at  $40^\circ\text{C}$  for 12 h. When a homogeneous solution was obtained, it was cast onto a glass plate using a doctor blade, and the THF solvent was evaporated at room temperature. It was further dried at  $80^\circ\text{C}$  under vacuum for 12 h. The obtained polymer electrolyte was a free-standing film with a thickness of 50 to  $60 \mu\text{m}$ , as shown in Fig. 1 and Fig. S1 (available online at [stacks.iop.org/JES/167/080525/mmedia](https://stacks.iop.org/JES/167/080525/mmedia)). Herein, the elastomeric polymer electrolyte (EPE) will be expressed as EPE-x, where x denotes the content of EMImTFSI as weight% in the polymer electrolyte.

**Electrode preparation and cell assembly.**—The  $\text{LiNi}_{0.6}\text{Co}_{0.2}\text{Mn}_{0.2}\text{O}_2$  (Umicore, NCM622) composite cathode was prepared by casting a viscous slurry containing NCM622, polymer electrolyte (EPE-25), and Super P carbon (MMM Co.) (70/20/10 by weight) in THF onto a carbon-coated aluminum foil. The polymer electrolyte was used as a  $\text{Li}^+$  ion conductor as well as a binder in the composite

\*Electrochemical Society Member.

<sup>z</sup>E-mail: [dongwonkim@hanyang.ac.kr](mailto:dongwonkim@hanyang.ac.kr)

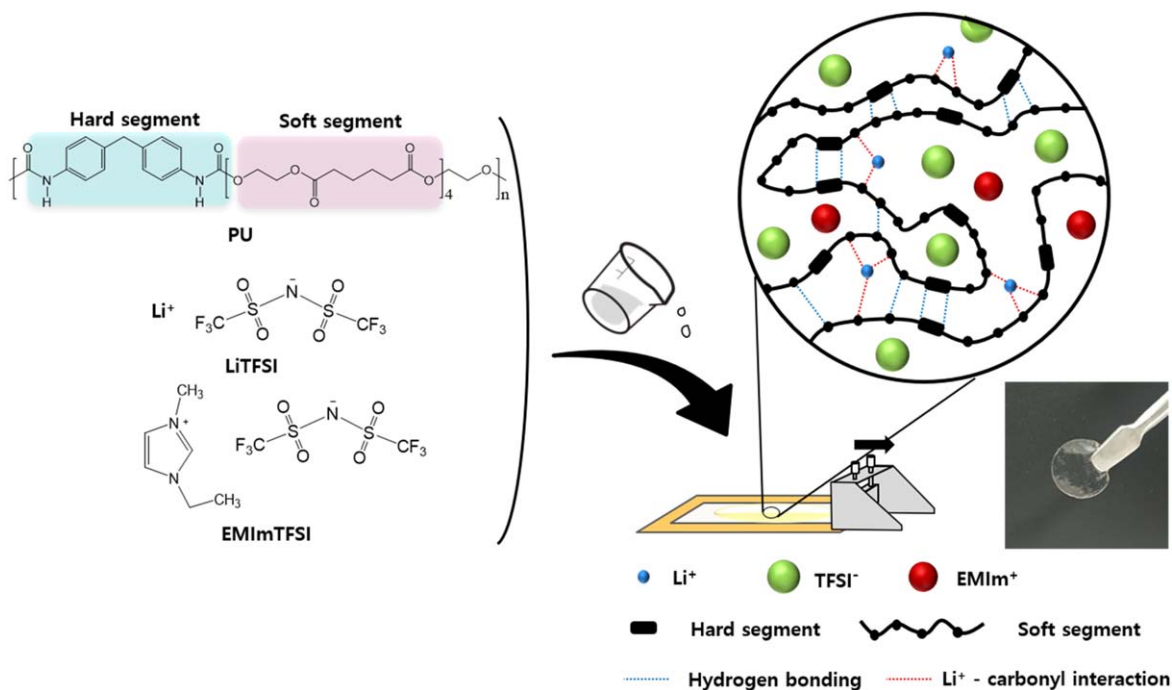


**Figure 1.** Schematic of the preparation of PU-based elastomeric polymer electrolyte and a photograph showing a free-standing film of EPE-25.

**Table I. Composition of PU-based elastomeric polymer electrolytes.**

Polymer electrolyte	PU (wt%)	LiTFSI (wt%)	EMImTFSI (wt%)
EPE-0	50.0	50.0	0
EPE-10	45.0	45.0	10
EPE-25	37.5	37.5	25
EPE-40	30.0	30.0	40

cathode. The electrode was dried under vacuum for 12 h at 80 °C and roll pressed to enhance the contact and adhesion to the current collector. The thickness of the composite cathode excluding the Al current collector was about 50  $\mu\text{m}$ . The areal density of active  $\text{LiNi}_{0.6}\text{Co}_{0.2}\text{Mn}_{0.2}\text{O}_2$  material in the composite cathode was about 8.0  $\text{mg cm}^{-2}$ . The lithium anode was prepared by pressing a lithium foil (200  $\mu\text{m}$ , Honjo Metal Co., Ltd.) onto a copper current collector. A Li/NCM622 cell was then assembled by sandwiching the polymer electrolyte film between the lithium anode and the NCM622 composite cathode in a CR2032-type coin cell. After cell assembly, the cells were kept at 55 °C for 24 h to improve the interfacial contacts between the elastomeric polymer electrolyte and the electrodes. For comparison, the Li/NCM622 cells were fabricated using a PE separator (Asahi ND 420, thickness: 20  $\mu\text{m}$ ) with ionic liquid electrolyte (0.5 M LiTFSI in EMImTFSI) or liquid electrolyte (1.15 M  $\text{LiPF}_6$  in EC/EMC/DEC (3:5:2 by volume) containing 2 wt% fluoroethylene carbonate). All the cells were assembled in a glove box filled with high-purity argon gas to avoid water and oxygen contamination.

**Characterization and measurements.**—Differential scanning calorimetry (DSC) measurements were performed using a TA instrument (SDT Q699/DSC Q20) with a heating rate of 5 °C  $\text{min}^{-1}$  from -80 to 120 °C under a dry nitrogen atmosphere. A thermogravimetric analyzer (TGA, SDT Q600/DSC Q20) was used to measure weight losses of PU and polymer electrolytes in the temperature range 50 °C–500 °C with a heating rate of 10 °C  $\text{min}^{-1}$  under the nitrogen atmosphere. The mechanical properties of polymer electrolyte film were measured using a universal testing machine (UTM) at a rate of 50  $\text{mm min}^{-1}$ . For ionic conductivity

measurements, the free-standing polymer electrolyte film was sandwiched between two stainless electrodes, and AC impedance measurements were performed using a Zahner Elektrik IM6 impedance analyzer in the frequency range of 10 Hz to 1 MHz with an amplitude of 10 mV at different temperatures. Each sample was allowed to equilibrate for 1 h before measurements. Linear sweep voltammetry (LSV) was carried out to investigate the electrochemical stability of the polymer electrolyte on a platinum working electrode, with lithium metal as the counter and reference electrodes, at a scanning rate of 1.0  $\text{mV s}^{-1}$  and 55 °C. The direct current (DC) polarization test of polymer electrolyte on Li metal was performed by galvanostatic periodic cycling of a symmetric Li/polymer electrolyte/Li cell at constant current density of 0.1  $\text{mA cm}^{-2}$  at 55 °C for 1 h during charge and discharge cycles, respectively. The lithium ion transference number ( $t^+$ ) in the polymer electrolyte was measured in the Li/polymer electrolyte/Li cell by using a combination of ac impedance and dc polarization measurements at 55 °C.<sup>37</sup> To investigate the interfacial stability of the polymer electrolyte with lithium electrode, the elastic polymer electrolyte was sandwiched between two lithium electrodes and sealed in coin cells. AC impedance measurements were performed in the frequency range from 100 mHz to 100 kHz at 55 °C. Galvanostatic cycling tests of the solid-state Li/NCM622 cell were conducted at a constant current rate of 0.2 C in the voltage range of 3.0 to 4.2 V at 55 °C using battery testing equipment (PNE). Morphological analysis of the lithium metal before and after cycling was performed using a scanning electron microscope (SEM, JEOL JSM-6300). Flammability tests were performed by igniting the polymer electrolyte with a flame torch.

## Results and Discussion

The thermal behavior of pristine PU and PU-based elastomeric polymer electrolytes was investigated by DSC analysis, and the resulting thermograms are shown in Fig. 2a. The glass transition temperature ( $T_g$ ) of pristine PU polymer was measured to be -44.9 °C without any melting peaks, indicating PU is a fully amorphous rubbery elastomer. When LiTFSI salt was added to the PU as in EPE-0, the  $T_g$  value increased to -32.8 °C.  $T_g$  values were also increased to -20.4 and -15.9 °C with addition of  $\text{LiBF}_4$  and

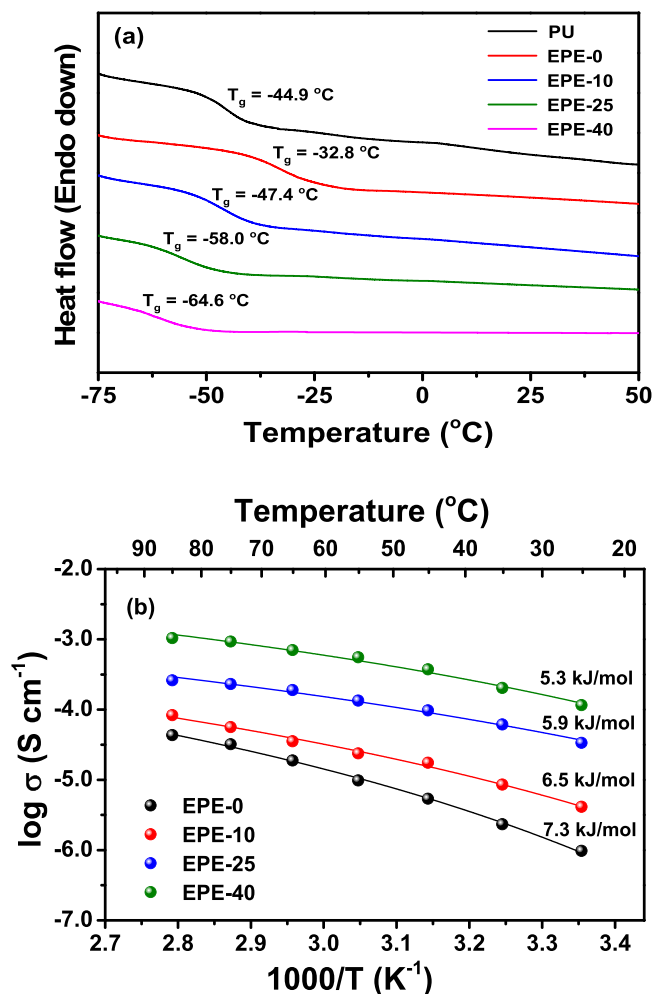


**Figure 2.** (a) DSC thermograms of PU and PU-based elastomeric polymer electrolytes containing different amounts of EMImTFSI. (b) Temperature dependence of the ionic conductivities of PU-based elastomeric polymer electrolytes containing different amounts of EMImTFSI. The symbols are experimental data, and the solid lines are VTF fitting results for ionic conductivities of the elastomeric polymer electrolytes.

LiClO<sub>4</sub>, respectively, as shown in Fig. S2. These phenomena can be attributed to occurrence of ion-dipole interactions between Li<sup>+</sup> ions and carbonyl groups in PU, as schematically illustrated in Fig. 1. These results suggest that PU polymer has good solvating properties for dissolving lithium salt and high chain flexibility with a low glass transition temperature. Despite the low *T<sub>g</sub>* of the amorphous rubbery film, the intermolecular hydrogen bonding between urethane groups resulted in high mechanical strength of the resulting polymer electrolyte film.<sup>28,38</sup> When EMImTFSI was added into the polymer electrolyte, *T<sub>g</sub>* gradually decreased to -64.6 °C at 40 wt% of EMImTFSI, indicating that addition of EMImTFSI into the polymer electrolyte improves the chain flexibility of the polymer backbone. Thus, EMImTFSI plays a role as a plasticizing additive. Figure 2b shows the temperature dependence of ionic conductivity of various polymer electrolytes in the temperature range of 25 °C to 85 °C. The ionic conductivity of the polymer electrolyte can be described by the Vogel–Tammann–Fulcher (VTF) Eq. 1,<sup>39</sup>

$$\sigma = AT^{-1/2} \exp[-E_a/R(T - T_0)] \quad [1]$$

where *A* is the pre-exponential factor, *E<sub>a</sub>* is the activation energy for conducting ions, and *T<sub>0</sub>* is the reference temperature that is normally 10–50 K below the glass transition temperature. This result reveals the contribution of segmental motion of the polymer chain for

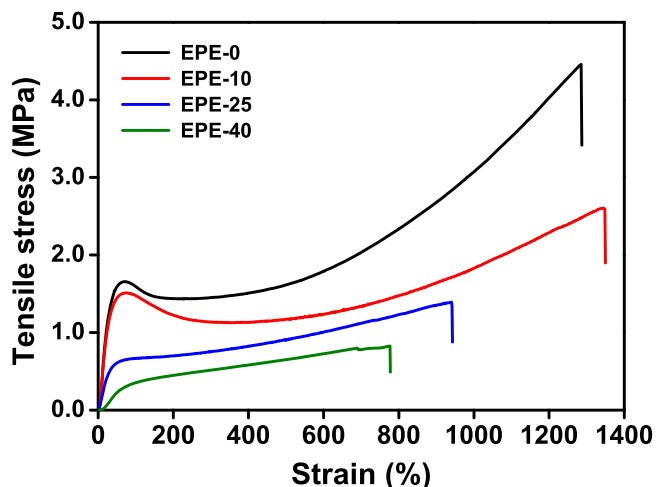


**Figure 3.** Stress-strain curves of various elastomeric polymer electrolyte films.

conducting ions in polymer electrolytes. As the content of EMImTFSI increased, the ionic conductivity of the polymer electrolytes increased, with a decrease in activation energy for ion conduction (*E<sub>a</sub>*). As discussed earlier, addition of EMImTFSI into the polymer electrolyte increases the segmental motions of the polymer chain, resulting in increase in ionic mobility and ionic conductivity.

The mechanical behaviors of the various polymer electrolyte films were investigated based on the stress-strain curves obtained using a universal testing machine, and the results are shown in Fig. 3. The PU-based polymer electrolyte without EMImTFSI (EPE-0) exhibited a tensile strength of 4.5 MPa and a very high elongation of 1291%. The high mechanical strength and elasticity can be attributed to the phase-separated structure of the hard and soft segments in the polyurethane backbone. Intermolecular hydrogen bonding in the hard segments serves as physical anchor site, providing a restorative force when the polymer electrolyte film was stretched. On the other hand, the soft segments consisting of polyester blocks were elongated when the film was stretched, resulting in the high elasticity of the PU-based polymer electrolyte. When 10 wt% EMImTFSI was added into the polymer electrolyte (EPE-10), it was stretched slightly more than EPE-0. With a further increase in EMImTFSI content, both tensile strength and elongation decreased, indicating a reduction in mechanical strength of the polymer electrolyte film due to the plasticizing effect of EMImTFSI.

The electrochemical stability of ionic liquid electrolyte and various elastomeric polymer electrolytes was investigated by linear sweep voltammetry (LSV), and the resulting linear sweep voltammograms are shown in Fig. 4. The LSV measurements were conducted at 55 °C due to the low ionic conductivity of EPE-0 at room temperature. As shown in the cathodic scan (Fig. 4a), onset of the reductive current of the ionic liquid electrolyte was observed around 1.7 V vs Li/Li<sup>+</sup>, which can be ascribed to the reductive decomposition of EMIm<sup>+</sup>.<sup>40</sup> The large and steep cathodic current observed at 0 V vs Li/Li<sup>+</sup> corresponds to reductive deposition of Li<sup>+</sup> ions onto the working electrode (Li<sup>+</sup> + e → Li). In the PU-based polymer electrolyte without EMImTFSI (EPE-0), there were no cathodic peaks until reduction of Li<sup>+</sup> ions around 0 V, indicating EPE-0 as reductively stable at low potential. However, the magnitude of reductive current at 0 V vs Li/Li<sup>+</sup> was small due to the low ionic conductivity of EPE-0. When a small amount of EMImTFSI was added into the PU-based elastomeric polymer electrolyte, the reductive decomposition of EMIm<sup>+</sup> was not observed prior to reduction of Li<sup>+</sup> ions. This result suggests that decomposition of EMIm<sup>+</sup> can be suppressed by encapsulating it in polymer matrix. As the content of EMImTFSI increased, the reduction of Li<sup>+</sup> ions at 0 V became easier due to the enhanced ion conduction in the polymer

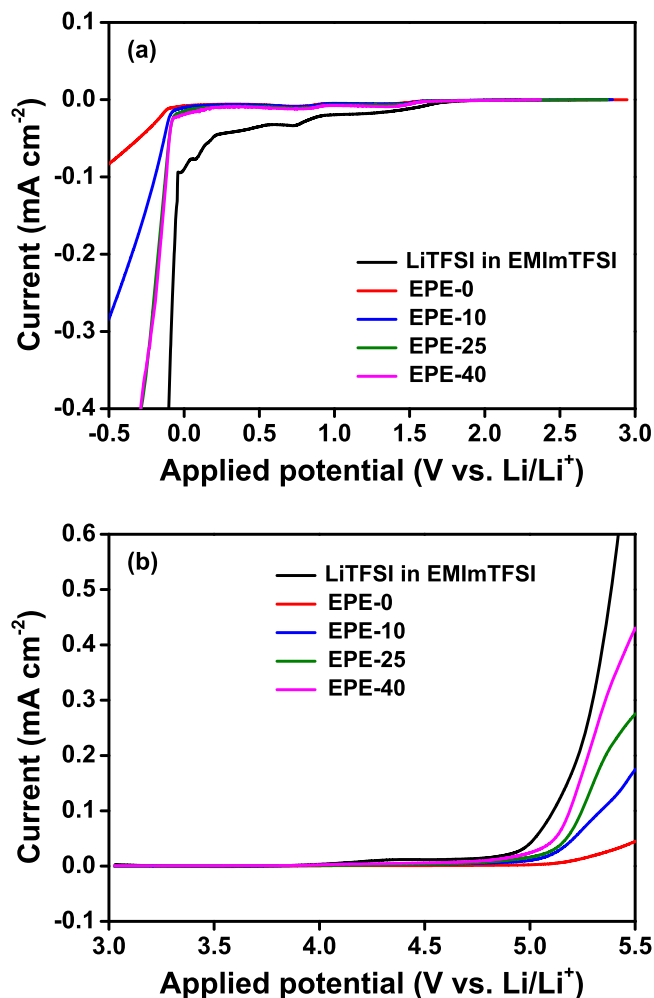


**Figure 4.** Linear sweep voltammograms of ionic liquid electrolyte (LiTFSI in EMImTFSI) and PU-based elastomeric polymer electrolytes at a scan rate of  $1 \text{ mV s}^{-1}$  and  $55^\circ\text{C}$ : (a) cathodic scan and (b) anodic scan.

electrolyte. As shown in the anodic scan in Fig. 4b, the oxidative stability of PU-based polymer electrolyte was enhanced compared to that of ionic liquid electrolyte. It should be noted that the anodic stability of PU-based polymer electrolyte decreased with increasing content of EMImTFSI. Cyclic voltammograms of the EPE-25 at  $55^\circ\text{C}$  are given in Fig. S3. The voltammograms revealed that the lithium deposition/stripping was reversible and no anodic current corresponding to the oxidative decomposition of polymer electrolyte could be observed up to  $4.2 \text{ V}$ . These results suggest that the polymer electrolytes investigated in this work are electrochemically stable, indicating that PU-based elastomeric polymer electrolytes can be applied to Li/NCM622 cells.

The repeated plating and stripping cycling behavior of the symmetrical Li/EPE-*x*/Li cells was investigated by DC polarization. Figure 5 depicts the voltage profiles of the Li/EPE-*x*/Li cells during stripping and plating of lithium, which were obtained at  $0.1 \text{ mA cm}^{-1}$  for 1 h and  $55^\circ\text{C}$  during plating and stripping cycles, respectively. All the Li/Li cells assembled with EPE-*x* showed stable voltage profiles, indicating even plating and stripping of lithium ( $\text{Li} \leftrightarrow \text{Li}^+ + \text{e}$ ), which can be attributed to the good interfacial contact between the elastomeric polymer electrolyte and lithium electrode as well as the interfacial stability of the polymer electrolyte toward the lithium electrode. These results demonstrate that the PU-based elastomeric polymer electrolytes on the lithium electrode provide a uniform current distribution to the electrolyte-electrode interface and suppress the growth of lithium dendrites during repeated

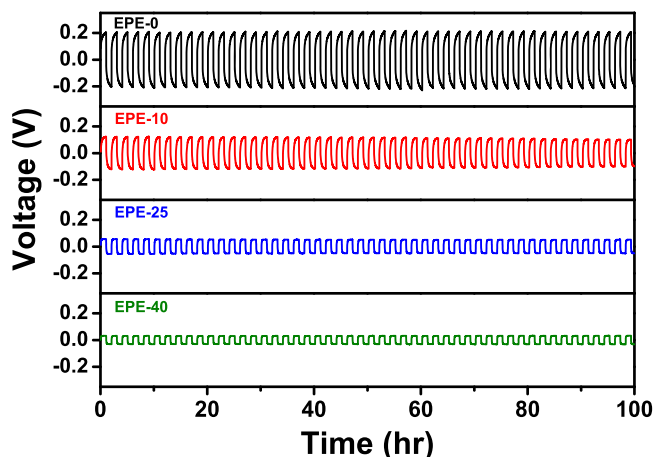


**Figure 5.** DC polarization voltage profiles of the symmetrical Li/EPE-*x*/Li cells at a current density of  $0.1 \text{ mA cm}^{-2}$  and  $55^\circ\text{C}$ .

cycling. Among the cells investigated, those employing the EPE-40 exhibited the lowest overpotential due to the low internal resistance of the cell. The above results confirmed that the EPE-40 electrolyte exhibited the highest ionic conductivity due its fully amorphous nature and high chain flexibility. However, it was difficult to prepare a dimensionally stable free-standing film using EPE-40. Accordingly, EPE-25 is likely the optimum polymer electrolyte system considering both the electrochemical properties and mechanical stability of the polymer electrolytes. The EPE-25 was a free-standing, flexible, rubbery film, as shown in Fig. 1. The interfacial stability of EPE-25 with lithium electrode was investigated by monitoring the AC impedance spectrum of the symmetric Li/EPE-25/Li cell as a function of storage time. Figure S4 shows the time evolution of AC impedance spectra of the symmetric Li cell at  $55^\circ\text{C}$ . The interfacial resistance ( $R_i$ ) corresponding to the diameter of semicircle increased initially and eventually stabilized after 4 days. The initial increase of  $R_i$  can be attributed to the gradual growth of a resistive layer on the lithium electrode. A steady-state value of  $R_i$  indicates good interfacial stability of the PU-based polymer electrolyte with lithium electrode. The lithium transference number in EPE-25 was measured by a combination of ac impedance and dc polarization measurements. From the data in Fig. S5, the lithium transference number in the PU-based elastomeric polymer electrolyte was estimated to be 0.33, indicating that the mobility of the  $\text{Li}^+$  ions is lower than that of the anions. This is due to the fact that the  $\text{Li}^+$  ions are strongly coordinated by the polymer chains through ion-dipole interactions, while the anions are loosely associated with the polymer segments.

A solid-state Li/NCM622 cell was assembled by sandwiching the elastomeric polymer electrolyte (EPE-25) between the Li anode and composite NCM622 cathode. The assembled Li/EPE-25/NCM622 cell was cycled at a constant current rate of  $0.2 \text{ C}$  at  $55^\circ\text{C}$ . Its typical charge and discharge curves are presented in Fig. 6a. Initially, the cell delivered a discharge capacity of  $149.3 \text{ mAh g}^{-1}$  based on NCM622 material in the composite cathode, with a coulombic efficiency of 93.5%. After repeated cycling, the overpotential was gradually increased with a decrease in discharge capacity. As a result, its discharge capacity decreased to  $122.3 \text{ mAh g}^{-1}$  after 100 cycles. The cycling performance of the Li/EPE-25/NCM622 cell was compared with that of the cell employing ionic liquid electrolyte (ILE) in Fig. 6b. The initial discharge capacity of the Li/ILE/NCM622 cell was slightly higher than that of the cell with EPE-25. However, the discharge capacity of the cell with ionic liquid electrolyte faded quickly with cycling and showed lower coulombic efficiencies than the Li/EPE-25/NCM622 cell throughout cycling. This result can be ascribed to the poor reductive stability of ionic liquid electrolyte at low potential on the lithium electrode, as

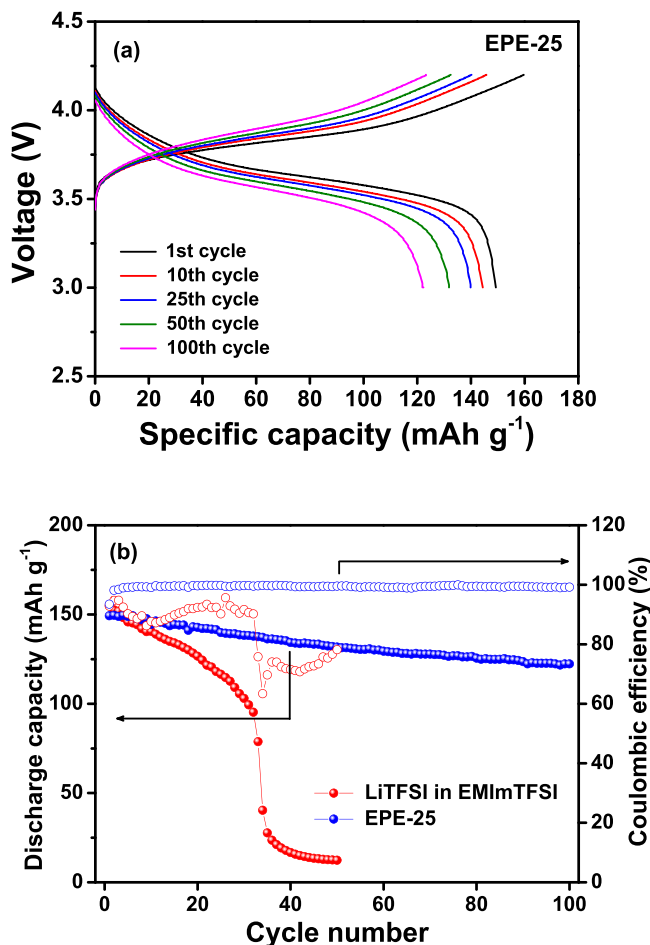


**Figure 6.** (a) Charge and discharge curves of the Li/NCM622 cell assembled with EPE-25 and (b) discharge capacities and coulombic efficiencies of Li/NCM622 cells with different electrolytes as a function of cycle number at 55 °C.

explained earlier. On the other hand, the cell with EPE-25 exhibited good cycling stability, and the coulombic efficiency of the cell remained higher than 99.4% throughout repeated cycles. The cycling performance of the solid-state Li/NCM622 cell was also compared with that of cell employing conventional liquid electrolyte in Fig. S6. The solid-state Li/NCM622 cell lost about 18.1% of its initial discharge capacity after 100 cycles, which is a larger capacity fading than that (10.1%) of liquid electrolyte-based cell. The capacity fading of the solid-state lithium cell may be related to the degradation of polymer electrolyte and the deterioration of interfacial contacts in the composite cathode. As previously reported,<sup>41,42</sup> the depolymerization of PU may be occurred by the presence of LiTFSI salt. Moreover, the adhesive property of PU as a binder in the composite cathode is not so strong enough as poly(vinylidene fluoride) to alleviate the mechanical stress in the composite cathode during the repeated cycling.

After repeated cycling, Li/NCM622 cells with different electrolytes were disassembled, and the morphologies of the lithium electrodes disassembled from the cells were investigated. As shown in Fig. 7b, the surface of the lithium electrode cycled in ionic liquid electrolyte exhibited a particulate dendrite morphology with large cracks. Since the ionic liquid electrolyte is reductively unstable toward the lithium electrode, decomposition products were deposited on the lithium metal, roughening the surface morphology. In contrast, the surface of the lithium electrode cycled in the elastomeric polymer electrolyte (EPE-25) showed a relatively flat surface without significant growth of lithium dendrites. As previously reported,<sup>43,44</sup> the use of polymer electrolyte with high elastic

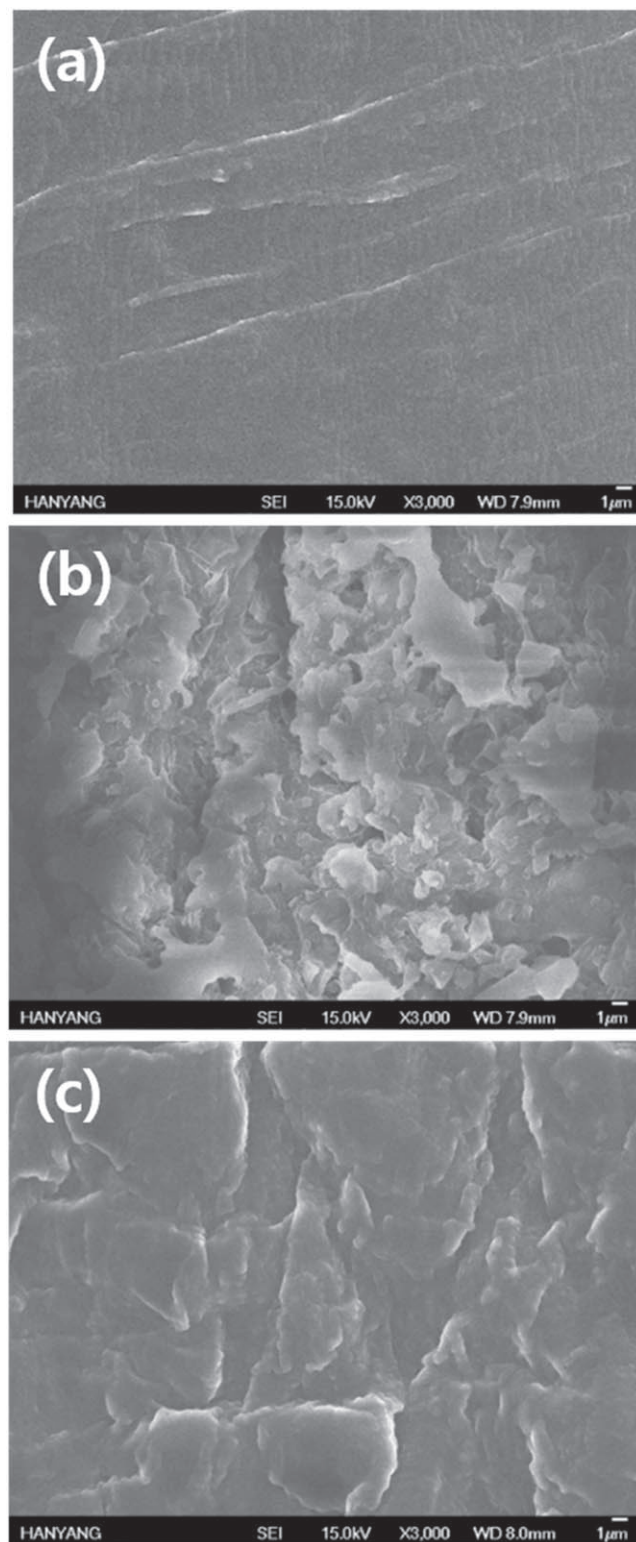


**Figure 7.** SEM images of (a) pristine lithium electrode, cycled lithium electrodes in (b) ionic liquid electrolyte (LiTFSI in EMImTFSI) and (c) elastomeric polymer electrolyte (EPE-25).

modulus can suppress growth of the lithium dendrites in two mechanisms. First, high compressive mechanical stress leads to reduced exchange current density at the protrusion peak compared to the valley. Second, plastic deformation of lithium metal results in reduction of the height of the dendritic protrusion. These results suggest that use of PU-based elastic polymer electrolyte allows

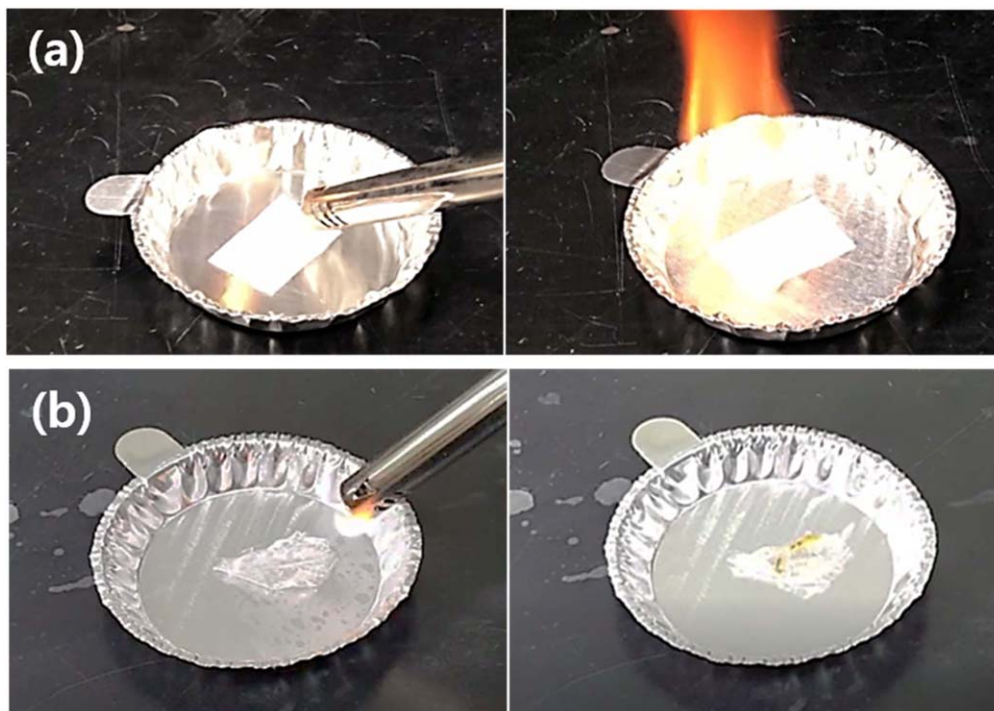


**Figure 8.** Photographic images of (a) PE separator soaked with liquid electrolyte and (b) PU-based elastomeric polymer electrolyte (EPE-25) during flammability test. Left side: during ignition with a flame source. Right side: after removing the flame source.

uniform deposition/dissolution of lithium on the surface of the lithium electrode and retards the lithium dendrite growth, which led to good cycling stability and high coulombic efficiency in the Li/EPE-25/NCM622 cells.

The flammability of the elastomeric polymer electrolyte (EPE-25) and PE separator wetted by a conventional carbonate-based liquid electrolyte were compared. The liquid electrolyte was 1.15 M LiPF<sub>6</sub> dissolved in ethylene carbonate (EC)/ethylmethyl carbonate (EMC)/diethyl carbonate (DEC)(3:5:2 by volume). Figure 8 shows the photographic images of two electrolyte systems obtained during flammability tests. As shown in Fig. 8a, the PE separator soaked with liquid electrolyte was highly flammable and burned after removing the flame source. In contrast, the PU-based elastomeric polymer electrolyte (EPE-25) did not show any combustion even during ignition with the flame source, which indicates its non-flammable behavior. The thermal stability of PU and PU-based elastomeric polymer electrolytes was examined by thermogravimetric analysis. As shown in Fig. S7, the thermal degradation of PU started around 295 °C due to the decomposition of the urethane bonds.<sup>45</sup> The addition of LiTFSI and EMImTFSI enhanced its thermal stability. The T<sub>d5</sub> (degradation temperature at 5% weight loss) of all the EPEs are above 296 °C, indicating that the PU-based elastomeric polymer electrolytes have sufficient thermal stability. This result suggests that employing PU-based elastomeric polymer electrolytes containing proper amounts of ionic liquid electrolyte allows fabrication of lithium metal polymer cells with high thermal stability.

### Conclusions

PU-based elastomeric polymer electrolytes were prepared as free-standing thin films, and their mechanical, thermal, and electrochemical properties were investigated for use in a Li/NCM622 cell. In addition to the high mechanical strength and electrochemical stability of PU-based elastomeric polymer electrolytes, addition of EMImTFSI improved the ionic conductivity of the polymer electrolyte. The Li/NCM622 cell assembled with the optimized elastomeric polymer electrolyte exhibited good cycling performance, while the non-flammable property of the

elastomeric polymer electrolyte allowed the fabrication of a Li/NCM622 cell with enhanced thermal safety.

### Acknowledgments

The authors gratefully acknowledge financial support from the Ministry of Trade, Industry, and Energy, Republic of Korea (10080314 and 20004958).

### ORCID

Dong-Won Kim  <https://orcid.org/0000-0002-1735-0272>

### References

1. M. Armand and J.-M. Tarascon, *Nature*, **451**, 652 (2008).
2. C. Liu, F. Li, M. L.- Peng, and H. M. Cheng, *Adv. Mater.*, **22**, 28 (2010).
3. J. B. Goodenough and K. S. Park, *J. Am. Chem. Soc.*, **135**, 1167 (2013).
4. R. Van Noorden, *Nature*, **507**, 26 (2014).
5. D. Larcher and J. M. Tarascon, *Nat. Chem.*, **7**, 19 (2015).
6. V. Etacheri, R. Marom, R. Elazari, G. Salitra, and D. Aurbach, *Energy Environ. Sci.*, **4**, 3243 (2011).
7. Y. Zhao, Y. Ding, Y. Li, L. Peng, H. R. Byon, J. B. Goodenough, and G. Yu, *Chem. Soc. Rev.*, **44**, 7968 (2015).
8. X. Judez, H. Zhang, C. Li, G. G. Eshetu, J. A. Gonzalez-Marcos, M. Armand, and L. M. Rodriguez-Martinez, *J. Electrochem. Soc.*, **165**, A6008 (2018).
9. L. Wang, Z. Wu, J. Zou, P. Gao, X. Niu, H. Li, and L. Chen, *Joule*, **3**, 2086 (2019).
10. X. Wang, R. Kerr, F. Chen, N. Goujon, J. M. Pringle, D. Mecerreyes, M. Forsyth, and P. C. Howlett, *Adv. Mater.*, **31**, 1905219 (2020).
11. Z. Hu, S. Zhang, S. Dong, W. Li, H. Li, G. Cui, and L. Chen, *Chem. Mater.*, **29**, 4682 (2017).
12. Z. Hu, S. Zhang, S. Dong, Q. Li, G. Cui, and L. Chen, *Chem. Mater.*, **30**, 4039 (2018).
13. I. S. Kang, Y.-S. Lee, and D.-W. Kim, *J. Electrochem. Soc.*, **161**, A53 (2014).
14. W.-K. Shin, A. G. Kannan, and D.-W. Kim, *ACS Appl. Mater. Interfaces*, **7**, 23700 (2015).
15. N. Delaporte, A. Guerfi, H. Demers, H. Lorrman, A. Paoletta, and K. Zaghib, *ChemistryOpen*, **8**, 192 (2019).
16. T. Jiang, P. He, G. Wang, Y. Shen, C.-W. Nan, and L.-Z. Fan, *Adv. Energy Mater.*, **10**, 1903376 (2020).
17. B. Zhang, L. Chen, J. Hu, Y. Liu, Y. Liu, Q. Feng, G. Zhu, and L.-Z. Fan, *J. Power Sources*, **442**, 227230 (2019).
18. S. Kaboli, H. Demers, A. Paoletta, A. Darwiche, M. Dontigny, D. Clement, A. Guerfi, M. L. Trudeau, J. B. Goodenough, and K. Zaghib, *Nano Lett.*, **20**, 1607 (2020).

19. B. Commarieu, A. Paoletta, J.-C. Daigle, and K. Zaghbi, *Curr. Opin. Electrochem.*, **9**, 56 (2018).
20. L. Chen, W. Li, L.-Z. Fan, C.-W. Nan, and Q. Zhang, *Adv. Funct. Mater.*, **29**, 1901047 (2019).
21. D. Fenton, J. Parker, and P. Wright, *Polymer*, **14**, 589 (1973).
22. F. Croce, G. B. Appetecchi, L. Persi, and B. Scrosati, *Nature*, **394**, 456 (1998).
23. J.-H. Shin, W. A. Henderson, and S. Passerini, *J. Electrochem. Soc.*, **152**, A978 (2005).
24. H. Zhang, C. Liu, L. Zheng, F. Xu, W. Feng, H. Li, X. Huang, M. Armand, J. Nie, and Z. Zhou, *Electrochim. Acta*, **133**, 529 (2014).
25. Y.-C. Jung, S.-M. Lee, J.-H. Choi, S. S. Jang, and D.-W. Kim, *J. Electrochem. Soc.*, **162**, A704 (2015).
26. D.-W. Kim, J.-S. Song, and J.-K. Park, *Electrochim. Acta*, **40**, 1697 (1995).
27. Y. C. Lee, M. A. Ratner, and D. F. Shriver, *Solid State Ionics*, **138**, 273 (2001).
28. C.-K. Lin and I. Der Wu, *Polymer*, **52**, 4106 (2011).
29. Y. Tominaga and K. Yamazaki, *Chem. Commun.*, **50**, 4448 (2014).
30. J. Mindemark, B. Sun, E. Torma, and D. Brandell, *J. Power Sources*, **298**, 166 (2015).
31. K. Deng, S. Wang, S. Ren, D. Han, M. Xiao, and Y. Meng, *ACS Appl. Mater. Interfaces*, **8**, 33642 (2016).
32. Y.-C. Jung, M.-S. Park, D.-H. Kim, M. Ue, A. Eftekhari, and D.-W. Kim, *Sci. Rep.*, **7**, 17482 (2017).
33. M.-S. Park, Y.-C. Jung, and D.-W. Kim, *Solid State Ionics*, **315**, 65 (2018).
34. J. Mindemark, M. J. Lacey, T. Bowden, and D. Brandell, *Prog. Polym. Sci.*, **81**, 114 (2018).
35. C. F. Francis, I. L. Kyratzis, and A. S. Best, *Adv. Mater.*, **32**, 1904205 (2020).
36. A. Mauger, C. M. Julien, A. Paoletta, M. Armand, and K. Zaghbi, *Mater. Sci. Eng. R*, **134**, 1 (2018).
37. J. Evans, C. A. Vincent, and P. G. Bruce, *Polymer*, **28**, 2324 (1987).
38. M.-S. Park, H.-S. Woo, J.-M. Heo, J.-M. Kim, R. Thangavel, Y.-S. Lee, and D.-W. Kim, *ChemSusChem*, **12**, 4645 (2019).
39. E. Quartarone and P. Mustarelli, *Chem. Soc. Rev.*, **40**, 2525 (2011).
40. M. Tulodziecki, J. M. Tarascon, P. L. Taberna, and C. Guery, *Electrochem. Commun.*, **77**, 128 (2017).
41. B. Commarieu, A. Paoletta, S. Collin-Martin, C. Gagnon, A. Vijn, A. Guerfi, and K. Zaghbi, *J. Power Sources*, **436**, 226852 (2019).
42. O. Akbulut, I. Taniguchi, S. Kumar, Y. Shao-Horn, and A. M. Mayes, *Electrochim. Acta*, **52**, 1983 (2007).
43. P. Barai, K. Higa, and V. Srinivasan, *Phys. Chem. Chem. Phys.*, **19**, 20493 (2017).
44. M. Golozar, P. Hovington, A. Paoletta, S. Bessette, M. Lagace, P. Bouchard, H. Demers, R. Gauvin, and K. Zaghbi, *Nano Lett.*, **18**, 7583 (2018).
45. J. Bao, G. Shi, C. Tao, C. Wang, C. Zhu, L. Cheng, G. Qian, and C. Chen, *J. Power Sources*, **389**, 84 (2018).